Hybrid Control Using Sliding Mode Control with Interval Type-2 Fuzzy Controller of a Doubly Fed Induction Generator for Wind Energy Conversion

Abdelghafour Herizi[1]*   Riyadh Rouabhi[1]

[1]*LGE Research Laboratory, Department of Electrical Engineering, Faculty of Technology,
University Mohamed Boudiaf of M'sila, BP 166 Ichbilia 28000, Algeria*
*Corresponding author's Email: abdelghafour.herizi@univ-msila.dz

Abstract: The efficiency of a wind turbine depends primarily on the power of the wind, the power curve of the turbine and the ability of the generator to respond to fluctuations in the wind. This article then proposes a robust control strategy of the doubly-fed induction generator applied in the wind energy conversion system, the active and reactive powers, which are generated by the DFIG will be decoupled by the orientation of the stator flux. The proposed control is combined between sliding mode control and type-2 fuzzy logic, this technique is robust to the modeling uncertainties of the generator and the wind generator, and which makes it possible to optimize energy production (efficiency). Finally, the performance of the system was tested and compared by simulation in terms of follow-up of instructions and the robustness with respect to the parameter variations of the DFIG. The results obtained show the interest of such a control in this system.

Keywords: Doubly fed induction generator, Wind power, Bidirectional converter, Sliding mode control, Type-2 fuzzy logic.

1. Introduction

Electric power is a crucial element of any socio-economic development. It has become in the daily life of populations, especially in developed countries, a necessity that cannot be done without.

In recent years, there has been an evolution in electricity generation based on wind power. This source of energy has developed especially given the diversity of exploitable areas and the relatively attractive cost [1].

Most of the wind turbines installed today are equipped with a doubly-fed induction machine (DFIM), this is due to several advantages: variable speed generation (± 30% around the speed of synchronism), decoupled control active and reactive powers, reduction of mechanical stresses and acoustic noise, improvement of power quality and low cost [2, 3]. This allows it to operate over a wide range of wind speeds, and to get the maximum possible power from it at each of its speeds. Its stator circuit is connected directly to the power grid, while its rotor circuit is connected to the grid through power converters. Since the power exchanged between the rotor and the grid is low, the cost of converters is reduced compared to that of a variable speed wind turbine powered by the stator. This is the main reason why this generator is found in the production of high powers. A second reason is the possibility of adjusting the voltage of the generator at the connection point [4].

But the DFIG is subject to many constraints, such as the effects of parametric uncertainties (due to heating, saturation, …) and the disturbance of the speed variation. These constraints could therefore divert the system from its optimal functioning [1, 5]. Therefore control should be concerned with robustness and performance. The control of this machine is a delicate operation because of this motor characterized by multi-variable, nonlinear dynamics, with parameters varying over time and with a strong coupling between the magnetic behavior and the mechanical part. Various control approaches have
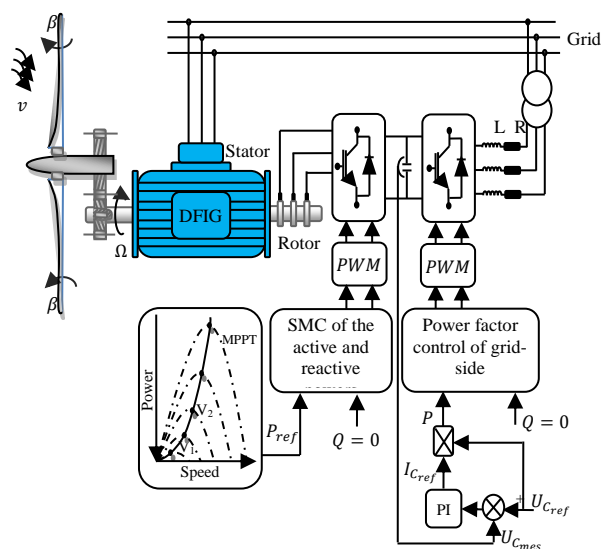
Figure. 1 Block diagram of the wind energy conversion system and its control

been exploited, we can non-exhaustively distinguish vector control, input-output linearization technique, sliding mode control, etc. [6, 7, 8].

The sliding mode control is part of the family of controllers with variable structure, i.e. controls switching between several different control laws. The importance of sliding mode controllers lies in: high precision, fast dynamic response, stability, simplicity of design and layout, and robustness to varying internal or external parameters. The principle of control by sliding modes is to force the trajectories of the system to reach a given surface, a sliding surface, in order to then stay there [9].

The SMC achieves robust control by adding a discontinuous control signal across the sliding surface, satisfying the sliding condition. Nevertheless, this type of control has an essential disadvantage, which is the chattering phenomenon caused by the discontinuous control action. Among the solutions proposed in the literature to remedy this drawback, there is the boundary layer method which consists in replacing the sign function by a continuous approximation in the vicinity of the sliding surface (saturation function or sigmoid function). Another method is to use higher order sliding modes, the principle of which is to reject discontinuities at the level of the upper derivatives of the input of the system. In order to reduce chattering, other methods can be applied, such as neural sliding control and sliding-fuzzy control [10-13].

La fuzzy logic theory forms an interface of the linguistic and digital worlds. She is able to describe complex systems by introducing vague information and by mimicking the approximate reasoning mechanism used in humans. A fuzzy controller can

be seen as a particular expert system having for objective to replace an operator qualified in his observation and his judgment, it then allows the treatment of often uncertain human ideas. There is a lot of interest in the fuzzy controller in controlling complex, nonlinear processes [14].

In the light of this observation, the main objective of this work is to develop optimal control method to improve the efficiency and productivity of the electric energy. This article is structured as follows: First, a dynamic model of the Wind energy conversion system was proposed. Then, a sliding mode control strategy of the doubly fed induction generator which allows independent control of the active and reactive power. In the fourth section, we synthesize a new control sliding mode with Interval type-2 fuzzy logic of DFIG. Finally, robustness tests of the proposed control will be carried out and comparative study with other controls.

2. Wind energy conversion system

For our system, the energy conversion chain consists of two converters on the rotor side.

The turbine transforms the kinetic power of the wind into mechanical power, but handiest part of the available power can be captured with the useful resource of the usage of the wind turbine [1]:

$$P = \frac{1}{2}\rho C_p S_v^3 \qquad (1)$$

For wind turbines, the C_p which relies upon on each the wind speed and rotational speed of the turbine is normally described withinside the variety 0.35-0.59 [15].

Thus, DFIG transforms mechanical energy into electric energy. As for the converter, it transfers the most energy brought with the aid of using the wind turbine to the community as a characteristic of the wind speed.

2.1 Modeling and control of the turbine

The turbine is made up of three-bladed rotor and a hub. Through the turbine, wind energy is transformed into mechanical energy that rotates the main shaft of the generator. The aerodynamic (mechanical) power P_m extracted by the wind turbine is given by [13]:

$$P_m = \frac{1}{2}\rho.\pi.R_T^2.V^3.C_p(\lambda, \beta) \qquad (2)$$

Where: ρ is the air density, R_T is the wind turbine rotor length and V is the wind speed.
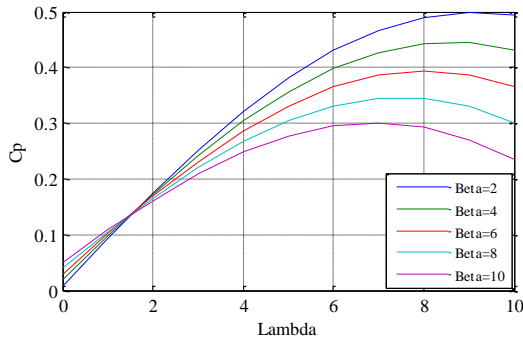
Figure. 2 Power coefficient C_p as a function of λ and β
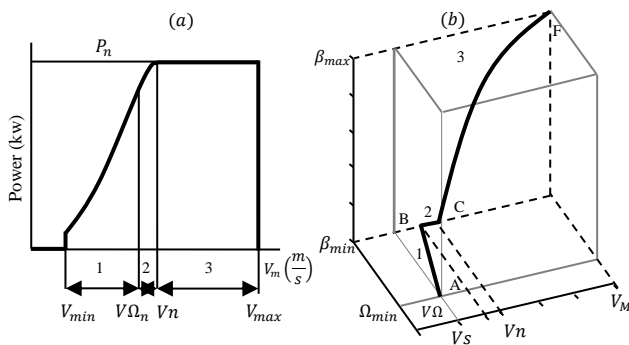
Figure. 3 Ideal characteristic of a wind turbine at variable speed [4]
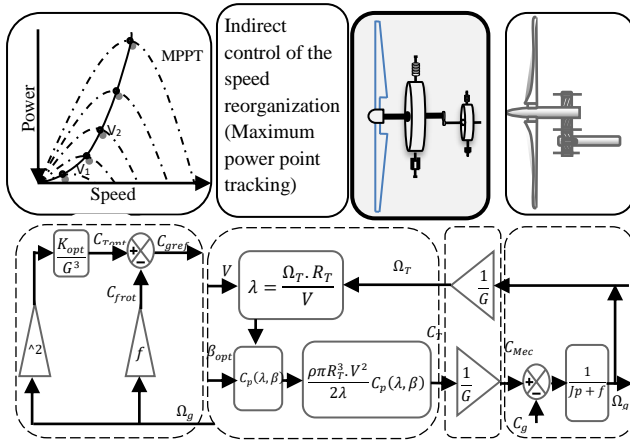
Figure. 4 Block diagram of the turbine and indirect control speed

The power coefficient $C_p(\lambda, \beta)$ represents the turbine efficiency to convert the kinetic energy of the wind into mechanical energy. This coefficient is a function of the blade pitch angle β and the tip speed ratio λ, which is defined as:

$$\lambda = \frac{\Omega_T . R_T}{V} \qquad (3)$$

Where: Ω_T is the shaft speed in (rad/s).

As a matter of example, the expression of the power coefficient of a wind turbine of 4Kw is approximated using the following equation:

$$C_p(\lambda, \beta) = \left(0,5 - 0,0167.(\beta - 2)\right). sin\left[\frac{\pi.(\lambda + 0,1)}{18,5 - 0,3.(\beta - 2)}\right] - 0,00184.$$
$$(\lambda - 3).(\beta - 2) \qquad (4)$$

Ideal characteristics of a wind turbine at variable speed are enumerated below [4]:
- Zone 1: corresponds to the low speed where wind is insufficient to actuate the wind system. The objective in this zone is to extract the maximum power of the wind by applying techniques called extraction of maximum power.
- Zone 2: In this zone, the speed of the wind is constant.
- Zone 3: corresponds to the very high speed of the wind. The objective in this zone is to limit the output power to the nominal power of the wind system to avoid overloads. This is done by action on the pitch angle of the blades.

In this zone of operation, the control has as main objective to maximize the captured energy of the wind and to minimize the efforts undergone by the driving mechanism. To maximize the capture of wind energy, there are two variables which are controlled in order to be maintained at their optimal values namely: λ_{opt}, β_{opt}. β is maintained by fixing the pitch angle at its optimal value β_{opt}, and λ by fixing the specific speed to its optimal value. The corresponding characteristic to this relation is given in zone 1, Fig. 3.

Optimization technique of the mechanical power used in this zone is the maximum power point tracking control (MPPT). In the present work, the maximum power coefficient is taken as: $C_{p\ max} = 0.48$ by achieving for a tip speed ratio of $\lambda_{opt} = 9.2$ and $\beta = 2$ deg. This choice has been dictated according to Fig. 2.

$$\begin{cases} C_{Topt} = \frac{1}{2}.\rho.\pi.R_T^3.V^2 \frac{C_p(\lambda_{opt})}{\lambda_{opt}} = k_{opt}\Omega_T^2 \\ V = \frac{\Omega_T.R_T}{\lambda_{opt}} \end{cases} \qquad (5)$$

With:

$$k_{opt} = \frac{1}{2}.\rho.\pi.R_T^5.\frac{C_p(\lambda_{opt})}{\lambda_{opt}^3} \; ; \frac{C_T}{G} - C_g - f.\Omega_g = 0 \; ;$$
$$\frac{k_{opt}}{G}.\Omega_T^2 - f.\Omega_g - C_g = 0 \; ; \Omega_g = G.\Omega_T;$$
$$C_{gopt} = \frac{k_{opt}}{G^3}.\Omega_g^2 - f.\Omega_g.$$

The block diagram given by Fig. 4 shows the implementation of the indirect control of the turbine.

2.2 Mathematical modelling of DFIG

The dynamic model of DFIG in (d, q) reference, which includes both the electrical and mechanical dynamics, can be described by the matrix form as follows [9, 16]:

$$\dot{X} = AX + BU \qquad (6)$$

Where:

$X = [\varphi_{sd} \quad \varphi_{sq} \quad I_{rd} \quad I_{rq}]^T$; $U = [V_{sd} \quad V_{sq} \quad V_{rd} \quad V_{rq}]^T$

$$[A] = \begin{bmatrix} -\frac{1}{T_s} & \omega_s & \frac{M}{T_s} & 0 \\ -\omega_s & -\frac{1}{T_s} & 0 & \frac{M}{T_s} \\ \alpha & -\beta\omega & -\delta & (\omega_s - \omega) \\ \beta\omega & \alpha & -(\omega_s - \omega) & -\delta \end{bmatrix} ;$$

$$[B] = \begin{bmatrix} 1 & 0 & 0 & 0 \\ 0 & 1 & 0 & 0 \\ -\frac{M}{\sigma L_s L_r} & 0 & \frac{1}{\sigma L_r} & 0 \\ 0 & -\frac{M}{\sigma L_s L_r} & 0 & \frac{1}{\sigma L_r} \end{bmatrix}$$

With: $\sigma = 1 - \frac{M^2}{L_r L_s}$; $T_r = \frac{L_r}{R_r}$; $T_s = \frac{L_s}{R_s}$; $\alpha = \frac{M}{\sigma L_r L_s T_s}$; $\beta = \frac{M}{\sigma L_r L_s}$; $\delta = \frac{1}{\sigma}\left(\frac{1}{T_r} + \frac{M^2}{L_s T_s L_r}\right)$

The mechanical and electromagnetic equations are given as follows:

$$J\frac{d\Omega}{dt} = C_{em} - C_r - f\Omega \qquad (7)$$

$$C_{em} = P\frac{M}{L_s}(\varphi_{sq} I_{rd} - \varphi_{sd} I_{rq}) \qquad (8)$$

With:

f coefficient of friction, J moment of inertia and P the number of pole pairs of the DFIG.

In order on the way to effortlessly control the power production of the wind turbine, an unbiased control of the energetic and reactive powers is finished with the aid of using setting up the equations which hyperlink the values of the rotor voltages to the energetic and reactive stator powers [2, 14].

By deciding on a (d, q) body of reference related to the rotating stator area and with the aid of using aligning the stator flux vector with the d axis, this effect in: $\varphi_{sd} = \varphi_s$ and $\varphi_{sq} = zero$.

If one supposes that the electric community is stable, that ends in φ_s constant. In addition, the stator resistance may be neglected. Based on those considerations, we achieve: $V_{sd} = zero$, $V_{sq} = V_s$ and $V_{sq} = V_s/\omega_s$.

Adapting the above equations to the simplifying assumptions gives:

$$\begin{cases} I_{sd} = \frac{\varphi_s}{L_s} - \frac{M}{L_s} I_{rd} \\ I_{sq} = -\frac{M}{L_s} I_{rq} \end{cases} \qquad (9)$$

$$\begin{cases} P_s = -\frac{V_s M}{L_s} I_{rq} \\ Q_s = \frac{V_s^2}{\omega_s L_s} - \frac{V_s M}{L_s} I_{rd} \end{cases} \qquad (10)$$

$$\begin{cases} \varphi_{rd} = \left(L_r - \frac{M^2}{L_s}\right) I_{rd} + \frac{V_s M}{\omega_s L_s} \\ \varphi_{rq} = \left(L_r - \frac{M^2}{L_s}\right) I_{rd} \end{cases} \qquad (11)$$

In this case the control voltages will be as follows:

$$V_{rd} = R_r I_{rd} + \left(L_r - \frac{M^2}{L_s}\right) \dot{I}_{rd} - g\omega_s \\ \left(L_r - \frac{M^2}{L_s}\right) I_{rq} \qquad (12)$$

$$V_{rq} = R_r I_{rq} + \left(L_r - \frac{M^2}{L_s}\right) \dot{I}_{rq} + g\omega_s \\ \left(L_r - \frac{M^2}{L_s}\right) I_{rd} + g\frac{V_s M}{L_s} \qquad (13)$$

With:

$\left(\frac{V_s M}{L_s}\right)$ the coupling term between the two axes;

$g\left(\frac{M^2}{L_s}\right)$ represents an electromotive force dependent on the speed of rotation.

The approach utilized in electrical control is to overlook the coupling phrases and installation an unbiased regulator on every axis, a good way to control the energetic electricity and the reactive electricity independently. This approach is known as the direct approach due to the fact electricity regulators at once control rotor voltages [1].

2.3 Modeling and control of the grid side converter

The grid side converter is used to provide bi-directed power flow from the rotor - side converter allowing the stabilization of the DC-link voltage and achieving unity power factor.

The AC source model and the rectifier model are given by the state space representation:

Figure. 5 Schematic diagram of grid side converter

Figure. 6 Block diagram of the grid side converter control

Figure. 7 Schematic diagram of rotor side converter

$$\begin{bmatrix} \dot{I}_1 \\ \dot{I}_2 \\ \dot{I}_3 \end{bmatrix} = \begin{bmatrix} \frac{-R}{L} & 0 & 0 \\ 0 & \frac{-R}{L} & 0 \\ 0 & 0 & \frac{-R}{L} \end{bmatrix} \begin{bmatrix} I_1 \\ I_2 \\ I_3 \end{bmatrix} + \frac{1}{L} \begin{bmatrix} V_1 - V_{An} \\ V_2 - V_{Bn} \\ V_3 - V_{Vn} \end{bmatrix} \quad (14)$$

The converter:

$$\begin{bmatrix} V_A \\ V_B \\ V_C \end{bmatrix} = \frac{U_c}{3} \cdot \begin{bmatrix} 2 & -1 & -1 \\ -1 & 2 & -1 \\ -1 & -1 & 2 \end{bmatrix} \begin{bmatrix} S_1 \\ S_2 \\ S_3 \end{bmatrix} \quad (15)$$

In addition, the rectified current is given by:

$$I_s = \begin{bmatrix} S_1 & S_2 & S_3 \end{bmatrix} \begin{bmatrix} I_1 \\ I_2 \\ I_3 \end{bmatrix} \quad (16)$$

The output voltage is governed by:

$$\begin{cases} \frac{dU_c}{dt} = \frac{1}{C} (I_s - I_{ch}) \\ U_C = R_{Ch}.I_{ch} \end{cases} \quad (17)$$

The objective of the grid side converter is to regulate the DC link voltage and to set at unity power factor.

The equations allowing the expression of the input AC voltage $V_p(d, q)$ to the rectifier in the (d, q) frame as a function of the voltages at the common connection point (CCP), $V(d, q)$ are given by the following equations:

$$\begin{aligned} V_{pd} &= V_d - RI_d - L\frac{dI_d}{dt} + L\omega I_q \\ V_{pq} &= V_q - RI_q - L\frac{dI_q}{dt} - L\omega I_d \end{aligned} \quad (18)$$

The real and reactive powers are expressed by:

$$\begin{cases} P = \frac{3}{2}.[V_d I_d + V_q I_q] \\ Q = \frac{3}{2}.[V_q I_d - V_d I_q] \end{cases} \quad (19)$$

Which can be rewritten in grouped form as follows:

$$\begin{bmatrix} P \\ Q \end{bmatrix} = \frac{3}{2}.\begin{bmatrix} V_d & V_q \\ V_q & -V_d \end{bmatrix} \begin{bmatrix} I_d \\ I_q \end{bmatrix} \quad (20)$$

Eq. (21) allows processing the reference currents (I_d^*, I_q^*) knowing the active and reactive powers references (P^*, Q^*).

$$\begin{bmatrix} I_d^* \\ I_q^* \end{bmatrix} = \frac{2}{3(V_d^2 + V_q^2)} \begin{bmatrix} V_d & V_q \\ V_q & -V_d \end{bmatrix} \begin{bmatrix} P^* \\ Q^* \end{bmatrix} \quad (21)$$

The reference of the real power P^* is calculated from the DC bus control loop responsible of maintaining constant DC capacitor voltage. Its value is given by the following expression:

$$\begin{cases} P^* = U_c I_s \\ Q^* = 0 \end{cases} \quad (22)$$

The rotor side converter is used to control the active and reactive powers injected by the stator of the doubly fed induction generator to the grid. The

used converter is a simple two level, three-phase inverter (Fig. 7).

The mathematical model of the rotor side converter is given by:

$$\begin{bmatrix} V_A \\ V_B \\ V_C \end{bmatrix} = \frac{E}{6} \cdot \begin{bmatrix} 2 & -1 & -1 \\ -1 & 2 & -1 \\ -1 & -1 & 2 \end{bmatrix} \begin{bmatrix} S_1 \\ S_2 \\ S_3 \end{bmatrix} \quad (23)$$

3. Sliding mode control

The primary concept of SMC is first to attract the states of the machine right into a certainly decided on the region, after which to lay out a control regulation with a view to usually hold the machine in that region [9, 17]. In summary, a SMC is split into 3 parts:

3.1 Choice of switching surface

For a non-linear system presented in the following form:

$$\dot{x} = f(x,t) + g(x,t).u(x,t)$$
$$x \in R^n, u \in R \quad (24)$$

Where: $f(x,t)$, $g(x,t)$ are continuous and unsure nonlinear functions, meant limited.

We take the shape of trendy equation given with the aid of using J. J. Slotine [18] to decide the sliding surface given with the aid of using:

$$s(x) = \left(\frac{d}{dt} + \lambda\right)^{n-1} e$$
$$e = x^d - x \quad (25)$$

Where: λ : positive coefficient; e : error on the signal to be adjusted; n : system order.

3.2 Convergence condition

The convergence situation is described with the aid of using the equation Lyapunov [19], it makes the region appealing and invariant.

$$s(x)\dot{s}(x) < 0 \quad (26)$$

3.2.1. Control calculation

The control set of rules is described with the aid of using the relation:

$$u = u^{eq} + u^n \quad (27)$$

Where:
u^{eq} : is the equal control vector, may be acquired with the aid of using thinking about the situation for the sliding regime;

u^n : is the switching part of the control (the correction factor).

In order to relieve the unwanted chattering phenomenon, J.J. Slotine proposed a method to lessen it, with the aid of using the "sign" function of the switching surface [18]. The switching a part of the control u^n is described with the aid of using:

$$u^n = k \, \text{sign}(s(x)) \quad (28)$$

With:
k is the controller gain.

3.2.2. Active power control

To control the active power, we take $n = 1$. The expression of the sliding surface becomes:

$$s(P) = \left(I_{rq}^{ref} - I_{rq}\right) \quad (29)$$

Its derivative is:

$$\dot{s}(P) = \left(\dot{I}_{rq}^{ref} - \dot{I}_{rq}\right) \quad (30)$$

By replacing the derivatives of the currents by their expressions given in Eqs. (10) and (13), we obtain:

$$\dot{s}(P) = \left(-\frac{L_s}{MV_s} \, \dot{P}_s^{ref} - \frac{1}{L_r\sigma}V_{rq} - \frac{1}{L_r\sigma}\left(-R_r I_{rq} - g\omega_s L_r \sigma I_{rd} - g\frac{MV_s}{L_s}\right)\right) \quad (31)$$

The control voltage V_{rq} is defined by: $V_{rq} = V_{rq}^{eq} + V_{rq}^n$. During the slip mode and in steady state, we have: $s(P) = 0$, $\dot{s}(P) = 0$ and $V_{rq}^n = 0$. Where we get from:

$$V_{rq}^{eq} = -\frac{L_s L_r \sigma}{MV_s} \, \dot{P}_s^{ref} + R_r I_{rq} + g\omega_s L_r \sigma I_{rd} + g\frac{MV_s}{L_s} \quad (32)$$

During the convergence mode, the condition $s(P)\dot{s}(P) < 0$ must be verified with:

$$V_{rq}^n = L_r \sigma k_1 \text{sign}(s(P)) \quad (33)$$

Where: $k_1 > 0$.

3.2.3. Reactive power control

In the same way as before, to control the reactive power we take $n = 1$. The expression of the sliding

surface becomes:

$$s(Q) = \left(I_{rd}^{ref} - I_{rd}\right) \qquad (34)$$

Its derivative is:

$$\dot{s}(Q) = \left(\dot{I}_{rd}^{ref} - \dot{I}_{rd}\right) \qquad (35)$$

By replacing $\dot{I}_{rd}^{ref}$ and $\dot{I}_{rd}$ by their expressions given by Eqs. (10) and (12), we obtain:

$$\dot{s}(Q) = \left(\left(\frac{V_s}{\omega_s M} - \frac{L_s}{V_s M}\dot{Q}_s^{ref}\right) - \frac{1}{L_r\sigma}V_{rd} - \right.$$
$$\left. \frac{1}{L_r\sigma}\left(-R_r I_{rd} + g\omega_s L_r\sigma I_{rq}\right)\right) \qquad (36)$$

The control voltage V_{rd} is defined by: $V_{rd} = V_{rd}^{eq} + V_{rd}^{n}$. During the slip mode and in steady state, we have: $s(Q) = 0$, $\dot{s}(Q) = 0$ and $V_{rd}^{n} = 0$. Where we get from:

$$V_{rd}^{eq} = L_r\sigma\left(\frac{V_s}{\omega_s M} - \frac{L_s}{V_s M}\dot{Q}_s^{ref}\right) + R_r I_{rd} -$$
$$g\omega_s L_r\sigma I_{rq} \qquad (37)$$

During the convergence mode, the condition $s(Q)\dot{s}(Q) < 0$ must be verified with:

$$V_{rd}^{n} = L_r\sigma k_2 \text{sign}\big(s(Q)\big) \qquad (38)$$

Where: k_2 positive constant.

4. Sliding mode control with interval type-2 FLC

4.1 Background of type-2 fuzzy logic

Type-2 FLCs give better results than their type-1 counterparts above all in environments full of uncertainties. The main characteristic of type-2 fuzzy sets is just their ability to handle uncertainties more efficiently than type-1 FLCs. This is possible because a larger number of parameters and more freedom degrees are available with type-2 fuzzy sets.

General structure of IT2FLCs is illustrated in Fig. 8. As it is clear, the structure is almost similar to the structure of T1FLCs. The main difference is that at least one of the FLCs in the rule base is an IT2FLC. Therefore, the outputs of the inference engine are IT2FLCs and a type reducer is needed in order to convert them into a T1FLC. Then, the T1FLCs is defuzzified into a crisp number as the output of the IT2FLC [20, 21].

4.1.1. Fuzzifier

The fuzzifier maps the crisp input vector $(x_1, x_2, ..., x_n)^T$ to a type-2 fuzzy system $\tilde{A}_x$, very similar to the procedure performed in a type-1 fuzzy logic system.

4.1.2. Rules

Consider a type-2 fuzzy logic system having inputs $x_1 \in X_1$, $x_2 \in X_2$, $x_n \in X_n$, and one output $y \in Y$. Let us suppose that it has M rules where the ith rule has the form:

$$R^i: \text{If } x_1 \text{ is } \tilde{F}_1^i \text{ and } x_2 \text{ is } \tilde{F}_2^i \text{ and } ... x_n \text{ is } \tilde{F}_n^i, \text{ than:}$$
$$y = \tilde{G}^i \qquad i = 1, ..., M \qquad (39)$$

Where: $\tilde{F}_j^i$ represent the type-2 fuzzy system of the input state j of the ith rule, $x_1, x_2, ..., x_n$ are the inputs, $\tilde{G}^i$ is the output of type-2 fuzzy system for the rule i, and M is the number of rules. As can be seen, the rule structure of type-2 fuzzy logic system is similar to type-1 fuzzy logic system except that type-1 membership functions are replaced with their type-2 counterparts.

4.1.3. Inference engine

In fuzzy system interval type-2 using the minimum or product t-norms operations, the ith activated rule $F^i(x_1, x_2, ..., x_n)$ gives us the interval that is determined by two extremes $\underline{f}^i(x_1, x_2, ..., x_n)$ and $\bar{f}^i(x_1, x_2, ..., x_n)$ [22]:

$$F^i(x_1, ..., x_n) =$$
$$\left[\underline{f}^i(x_1, ..., x_n), \bar{f}^i(x_1, ..., x_n)\right] \equiv \left[\underline{f}^i, \bar{f}^i\right] \qquad (40)$$

With: $\underline{f}^i$ and $\bar{f}^i$ are given as:

$$\underline{f}^i = \underline{\mu}_{F_1^i}(x_1) \times ... \times \underline{\mu}_{F_n^i}(x_n)$$
$$\bar{f}^i = \overline{\mu}_{F_1^i}(x_1) \times ... \times \overline{\mu}_{F_n^i}(x_n) \qquad (41)$$

4.1.4. Type reducer

After the rules are fired and inference is executed, the obtained type-2 fuzzy system, resulting in type-1 fuzzy system is computed. In this part, the available methods to compute the centroid of type-2 fuzzy system using the extension principle [23] are discussed. The centroid of type-1 fuzzy system A is given by:

$$C_A = \frac{\sum_{i=1}^{n} z_i w_i}{\sum_{i=1}^{n} w_i} \qquad (42)$$
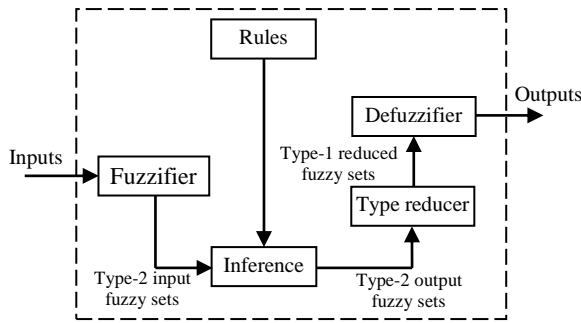
Figure. 8 Structure of type-2 fuzzy logic system [21]
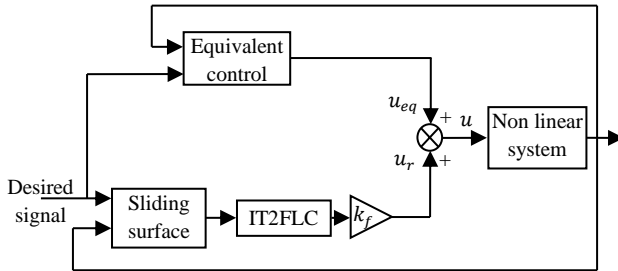
Figure. 9 Block diagram of the IT2FSMC

Where: n represents the number of discretized domain of A, $z_i \in R$ and $w_i \in [0,1]$.

If each z_i and w_i are replaced with a type-1 fuzzy system, Z_i and W_i, with associated membership functions of $\mu_Z(Z_i)$ and $\mu_W(W_i)$ respectively, by using the extension principle, the generalized centroid for type-2 fuzzy system $\tilde{A}$ is given by:

$$GC_{\tilde{A}} = \int_{z_1 \in Z_1} \cdots \int_{z_n \in Z_n} \int_{w_1 \in W_1} \cdots$$
$$\int_{w_n \in W_n} \frac{T_{i=1}^n \mu_Z(Z_i) \times T_{i=1}^n \mu_W(W_i)}{\frac{\sum_{i=1}^n z_i w_i}{\sum_{i=1}^n w_i}} \quad (43)$$

Where: T is a t-norm and $GC_{\tilde{A}}$ is a type-1 fuzzy system. For an interval type-2 fuzzy system:

$$GC_{\tilde{A}} = [y_l(x), y_r(x)]$$
$$= \int_{y^1 \in [y_l^1, y_r^1]} \cdots \int_{y^M \in [y_l^M, y_r^M]} \int_{f^1 \in [\underline{f}^1, \overline{f}^1]} \cdots$$
$$\int_{f^M \in [\underline{f}^M, \overline{f}^M]} \frac{1}{\frac{\sum_{i=1}^M f^i y^i}{\sum_{i=1}^M f^i}} \quad (44)$$

4.1.5. Deffuzzifier

To get a crisp output from a type-1 fuzzy logic system, the type-reduced set must be defuzzied. The most common method to do this is to find the centroid of the type-reduced set.

If the type-reduced set Y is discretized to n points, then the following expression gives the centroid of the type-reduced set as:

$$Y(x) = \frac{\sum_{i=1}^M y^i \mu(y^i)}{\sum_{i=1}^M \mu(y^i)} \quad (45)$$

We can compute the output using the iterative Karnik Mendel Algorithms [24]. Therefore, the defuzzified output of an interval type-2 FLC is:

$$Y(x) = \frac{y_l(x) + y_r(x)}{2} \quad (46)$$

With:

$$\begin{cases} y_l(x) = \frac{\sum_{i=1}^M f_l^i y_l^i}{\sum_{i=1}^M f_l^i} \\ y_r(x) = \frac{\sum_{i=1}^M f_r^i y_r^i}{\sum_{i=1}^M f_r^i} \end{cases} \quad (47)$$

The structure of a fuzzy system Type-2 is shown in the Fig. 8.

4.2 Sliding mode control - interval type 2 FLC of a DFIG

This section presents the design of a new nonlinear drive for the doubly fed induction generator. The proposed control is designed from the sliding mode control technique supplemented by a type-2 fuzzy controller to improve its robustness.

The control algorithms based on sliding mode techniques suffers from a main disadvantage that is chattering effect, which is the high frequency oscillation of the controller output. To overcome this problem and in order to reduce the chattering phenomenon, an interval type-2 fuzzy system is used to approximate the hitting control term. The configuration of the proposed type-2 fuzzy sliding mode control scheme is shown in Fig. 9; it contains an equivalent control part and single input single output interval type-2 fuzzy logic.

4.2.1. Development of a fuzzy controller of a DFIG

The equivalent control u_{eq}, is calculated in such a way as to have $\dot{s} = 0$. Then the discontinuous control is computed by:

$$u_r = k_f u_f \quad (48)$$

Where:

$$u_f = IT2FLC(s) \quad (49)$$

With:
k_f is the normalization factor of the output variable, and u_f is the output of the IT2FLC, which is obtained
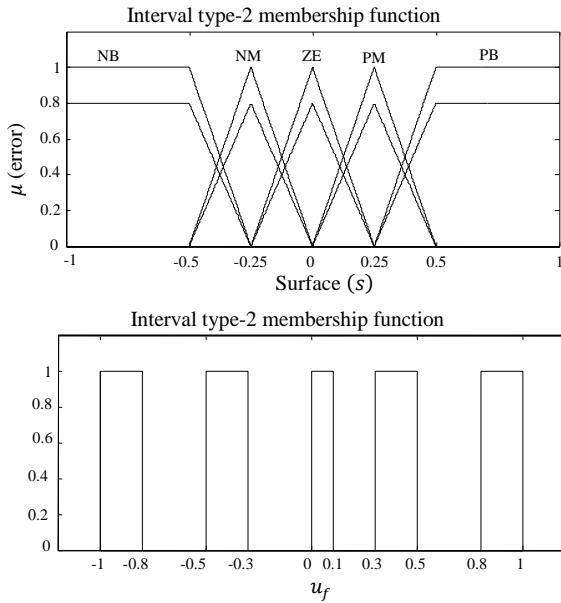
Figure. 10 Membership functions of input and output

Table.1. Fuzzy rules for type-2 FLCs

	Rule 1	Rule 2	Rule 3	Rule 4	Rule 5
s	PB	PM	ZE	NM	NB
u_f	NB	NM	ZE	PM	PB

by the normalized s.

The hybrid control sliding mode control-type 2 fuzzy controller (IT2FSMC) developed in this work given the following equations:

$$\begin{cases} V_{rq}^{ref} = V_{rq}^{eq} + V_{rq}^{n} \\ V_{rq}^{n} = \sigma L_r\big(k_{f1}u_f\big) \end{cases} \quad (50)$$

and

$$\begin{cases} V_{rd}^{ref} = V_{rd}^{eq} + V_{rd}^{n} \\ V_{rd}^{n} = \sigma L_r\big(k_{f2}u_f\big) \end{cases} \quad (51)$$

4.2.2. Interval type-2 fuzzy logic control

The fuzzy type-2 membership functions of the input sliding surface (s) and the output discontinuous control (u_f) sets are presented in Fig. 10.

In order to attenuate the chattering effect and handle the uncertainty of the modeling of the DFIM, a type-2 fuzzy controller has been used with single input and single output for each subsystem. Then, the input of the controller is the sliding surface and the output is the discontinuous control u_f. All the membership functions of the fuzzy input variable are chosen to be triangular and trapezoidal for all upper and lower membership functions. The used labels of

the fuzzy variable (surface) are: {negative medium (NM), negative big (NB), zero (ZE), positive medium (NM), positive big (PB)}.

The corrective control is decomposed into five levels represented by a set of linguistic variables: negative big (NB), negative medium (NM), zero (ZE), positive medium (PM) and positive big (PB). Table.1 presents the rules base which contains five rules:

The membership functions of the input (sliding surface) and output (u_f) has been normalized in the interval $[-1, 1]$, therefore: $|u_f| \leq 1$.

u_f given in Eq. (49) satisfies the following condition:

$$u_f = -k^+|s| \quad (52)$$

Where:
$k^+ > 0$ is positive constant determined by a fuzzy type-2 inference system.

Proof:

The discontinuous control laws are computed by type-2 fuzzy logic inference using Eqs (46) and (47) and the iterative Karnik Mendel Algorithms presented in [25, 26, 27]. Where $\alpha_i = [\alpha_{ilow}, \alpha_{iup}]$ for $i = [1, \dots, 5]$ are the membership interval of rules 1 to 5 presented in Table 1. Moreover, u_f can be further analyzed as the following six conditions given thereafter. Only one of six conditions will occur for any value of the error e according to Fig. 9.

Condition 1:

Only rule 1 is activated $\big(s > 0.5, \alpha_1 = [0.8, 1], \alpha_j = [0,0]\big)$ for $j = 2,3,4,5$.

$$u_f = IT2FLC(s) = \frac{-0.8 - 1}{2} = -0.9 \quad (53)$$

Condition 2:

Rule 1 and 2 are activated $\big(0.25 < s < 0.5, \alpha_1 = [\alpha_{1low}, \alpha_{1up}], \alpha_2 = [\alpha_{2low}, \alpha_{2up}], \alpha_j = [0,0]\big)$ for $j = 3,4,5$.
$0 \leq \alpha_{1low}, \alpha_{2low} \leq 0.8$ and $0 \leq \alpha_{1up}, \alpha_{2up} \leq 1$

$$u_f = IT2FLC(s) = \frac{1}{2}\left(\frac{-0.8\,\alpha_{1low} - 0.3\,\alpha_{2up}}{\alpha_{1low} + \alpha_{2up}} + \frac{-\alpha_{1up} - 0.5\,\alpha_{2low}}{\alpha_{1up} + \alpha_{2low}} \right) \quad (54)$$

Condition 3:

Rule 2 and 3 are activated $\big(0 < s < 0.25, \alpha_2 = [\alpha_{2low}, \alpha_{2up}], \alpha_3 = [\alpha_{3low}, \alpha_{3up}], \alpha_j = [0,0]\big)$ for $j = 1,4,5$.
$0 \leq \alpha_{2low}, \alpha_{3low} \leq 0.8$ and $0 \leq \alpha_{2up}, \alpha_{3up} \leq 1$
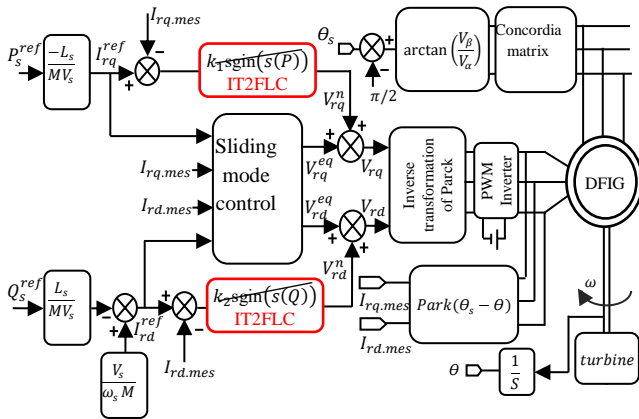
Figure. 11 Block diagram of the interval type-2 fuzzy sliding mode control of a DFIG

$$u_f = IT2FLC(s) = \frac{1}{2}\left(\frac{-0.3\,\alpha_{2low}+0.1\,\alpha_{3up}}{\alpha_{2low}+\alpha_{3up}} + \frac{-0.5\,\alpha_{2up}}{\alpha_{2up}+\alpha_{3low}}\right) \quad (55)$$

Condition 4:
Rule 3 and 4 are activated $\left(-0.25 < s < 0, \alpha_3 = [\alpha_{3low}, \alpha_{3up}], \alpha_4 = [\alpha_{4low}, \alpha_{4up}], \alpha_j = [0,0]\right)$ for $j = 1,2,5$.
$0 \le \alpha_{3low}, \alpha_{4low} \le 0.8$ and $0 \le \alpha_{3up}, \alpha_{4up} \le 1$

$$u_f = IT2FLC(s) = \frac{1}{2}\left(\frac{0.1\,\alpha_{3low}+0.5\,\alpha_{4up}}{\alpha_{3low}+\alpha_{4up}} + \frac{0.3\,\alpha_{4low}}{\alpha_{3up}+\alpha_{4low}}\right) \quad (56)$$

Condition 5:
Rule 4 and 5 are activated $\left(-0.5 < s < -0.25, \alpha_4 = [\alpha_{4low}, \alpha_{4up}], \alpha_5 = [\alpha_{5low}, \alpha_{5up}], \alpha_j = [0,0]\right)$ for $j = 1,2,3$.
$0 \le \alpha_{4low}, \alpha_{5low} \le 0.8$ and $0 \le \alpha_{4up}, \alpha_{5up} \le 1$

$$u_f = IT2FLC(s) = \frac{1}{2}\left(\frac{0.5\,\alpha_{4low}+\alpha_{5up}}{\alpha_{4low}+\alpha_{5up}} + \frac{0.3\,\alpha_{4up}+0.8\,\alpha_{5low}}{\alpha_{4up}+\alpha_{5low}}\right) \quad (57)$$

Condition 6:
Only rule 5 is activated $\left(s < -0.5, \alpha_5 = [0.8,1], \alpha_j = [0,0]\right)$ for $j = 1,2,3,4$.

$$u_f = IT2FLC(s) = \frac{1+0.8}{2} = 0.9 \quad (58)$$

According to six possible conditions shown in Eqs. (53-58) we conclude:

$$u_f = IT2FLC(s) = -k^+|s| \quad (59)$$

With:

$$k^+ = \begin{cases} 0.9 \\ if \quad s > \frac{1}{2} \ \& \ s < \frac{-1}{2} \\ \left|\frac{1}{2}\left(\frac{-0.8\,\alpha_{1low}-0.3\,\alpha_{2up}}{\alpha_{1low}+\alpha_{2up}} + \frac{-\alpha_{1up}-0.5\,\alpha_{2low}}{\alpha_{1up}+\alpha_{2low}}\right)\right| \\ if \quad \frac{1}{4} < s < \frac{1}{2} \\ \left|\frac{1}{2}\left(\frac{-0.3\,\alpha_{2low}+0.1\,\alpha_{3up}}{\alpha_{2low}+\alpha_{3up}} + \frac{-0.5\,\alpha_{2up}}{\alpha_{2up}+\alpha_{3low}}\right)\right| \\ if \quad 0 < s < \frac{1}{4} \\ \left|\frac{1}{2}\left(\frac{0.1\,\alpha_{3low}+0.5\,\alpha_{4up}}{\alpha_{3low}+\alpha_{4up}} + \frac{0.3\,\alpha_{4low}}{\alpha_{3up}+\alpha_{4low}}\right)\right| \\ if \quad \frac{-1}{4} < s < 0 \\ \left|\frac{1}{2}\left(\frac{0.5\,\alpha_{4low}+\alpha_{5up}}{\alpha_{4low}+\alpha_{5up}} + \frac{0.3\,\alpha_{4up}+0.8\,\alpha_{5low}}{\alpha_{4up}+\alpha_{5low}}\right)\right| \\ if \quad \frac{-1}{2} < s < \frac{-1}{4} \end{cases}$$

$$(60)$$

The block diagram of the interval type-2 fuzzy sliding mode control (IT2FSMC) is presented in Fig. 11. The first step of the control is to generate the currents of I_{rq}^{ref} and I_{rd}^{ref}, representing the dummy control. The error between these references and the real quantities of the currents results from new errors. Finally, we adapt the control law V_{rq}^{ref} and V_{rd}^{ref} from the Eqs. (50) and (51) to ensure the stability of the machine.

5. Simulation results

In order to show the performances and the robustness of the proposed IT2FSMC, we made a series of tests.

A. Follow-up of instructions

The first test consists in carrying out steps of active and reactive power.
For the reference active power:
- $t \in [0, 1]$: power step equals 0.
- $t \in [1, 3]$: power step equals -3000.
- $t \in [3, 5]$: power step equals 0.

For the reference reactive power:
- $t \in [0, 2]$: power step equals 0.
- $t \in [2, 4]$: power step equals 1000.
- $t \in [4, 5]$: power step equals 0.

B. Performances

This test allows us to verify the extent to which the active and reactive powers follow their
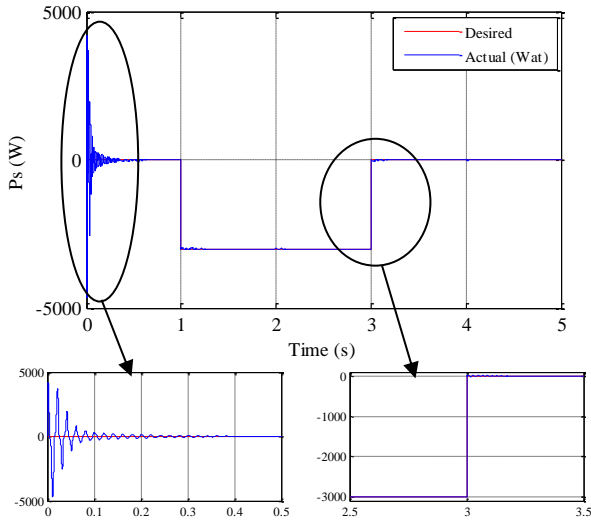
Figure. 12 Simulation result of active power P_s
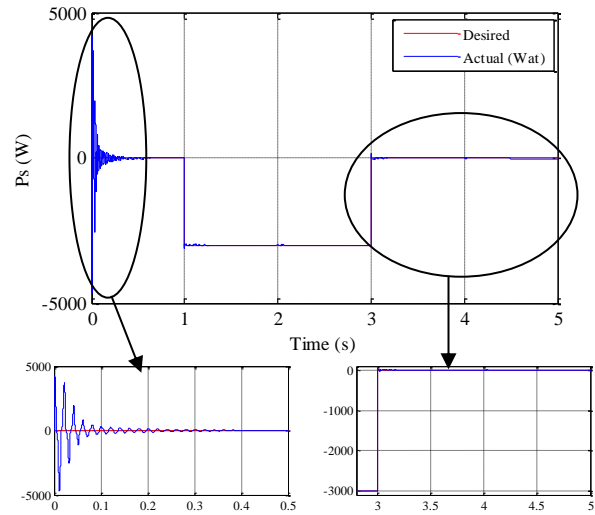
Figure. 14 Simulation result of P_s with a change in machine speed
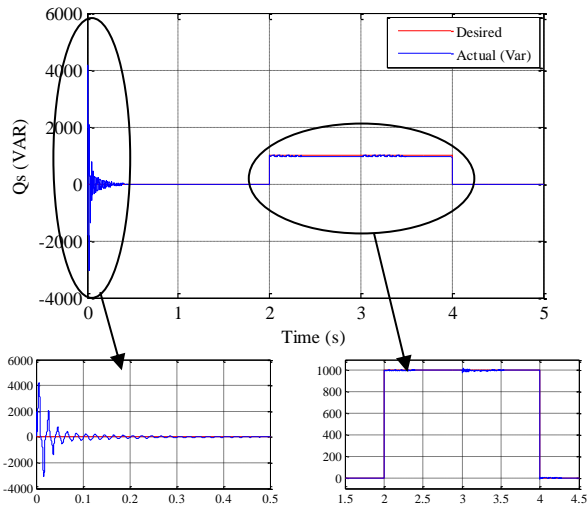
Figure. 13 Simulation result of reactive power Q_s
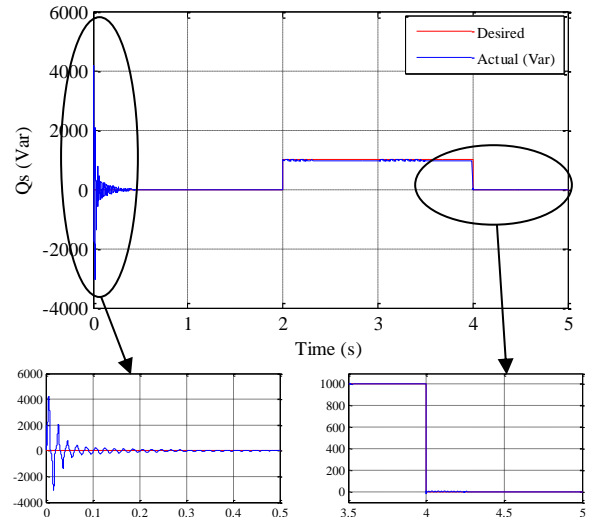
Figure. 15 Simulation result of Q_s with a change in machine speed

instructions when the rotational speed of the machine suddenly varies at the instant t = 4.5 and goes from 1440 rpm to 1600 rpm. We notice: Active power equals with zoom -8 W and reactive power equals with zoom 0.2 VAR.

From the simulation results shown in Figs. 12-15 we can observe that the proposed control technique allows a perfect decoupling between the two components of the P_s and Q_s stator power, it appears clearly that the new control present positive performances compared to the traditional controls (vector control and sliding mode) and new controls as found in reference [9] and [17], namely: the tracking errors are low with acceptable overshoots, the response times which characterize the transient regime are low.

In general, the simulation results obtained during the application of the IT2FSMC show good tracking

of the powers generated at the corresponding reference values.

6. Performance comparison

In the present study includes four criteria of static error e (speed and flux). These criteria are integrated squared error (ISE), integral absolute error (IAE), integral time-weighted squared error ($ITSE$) and integral time-weighted absolute error ($ITAE$), are utilized to judge the performance of the controllers. The index ISE, IAE, $ITSE$ and $ITAE$ is expressed as follows:

$$ISE = \int_0^T e^2(t)dt \qquad (61)$$

560

Table 2. ISE, IAE, $ITSE$ and $ITAE$ performance indexes

Control Index		Fuzzy sliding [9]	Neural sliding [17]	IT2FSMC Proposed
ISE	P_s	2,5446×10⁵	4,7534×10⁵	2,0936×10⁵
	Q_s	1,5177×10⁵	4,8736×10⁵	1,1514×10⁵
IAE	P_s	163,9519	110,7065	139,2916
	Q_s	93,6977	106,4587	87,1864
$ITSE$	P_s	5,3007×10³	3,2221×10⁴	4,7193×10³
	Q_s	2,5447×10³	3,8491×10⁴	2,0857×10³
$ITAE$	P_s	84,0344	97,3149	88,4425
	Q_s	20,6390	23,4804	18,3652

$$IAE = \int_0^T |e(t)| dt \qquad (62)$$

$$ITSE = \int_0^T t.e^2(t) dt \qquad (63)$$

$$ITAE = \int_0^T t|e(t)| dt \qquad (64)$$

The objective of this part is to compare the different control laws synthesized, the fuzzy sliding mode control proposed in [9], neural sliding mode control proposed in [17] and the proposed controller.

Table 2 shows the ISE, IAE, $ITSE$ and $ITAE$ values of the simulation results. Actually, these performance indices are obtained at the end of the simulation time (T = 5sec) with a sampling period h=10⁻⁴. From the comparison, it can be seen that the performance is improved when using the proposed controller as compared to the anther methods.

The results presented in the table above clearly show that the proposed control (IT2FSMC) is the most efficient from the point of view of minimizing the energy criterion ISE, IAE, $ITSE$ and $ITAE$.

7. Conclusion

In this article, it was presented the control of a wind power conversion system equipped with a dual power asynchronous generator.

After modeling the system, we developed two controllers one for active power and the other for reactive power, using interval type-2 fuzzy controller with sliding mode control.

With an appropriate choice of controller parameters, the results we have obtained are interesting for the application of wind energy to ensure the robustness and quality of the energy produced.

In addition, this control has a simple and robust control algorithm which has the advantage of being easily implantable in a computer.

8. Appendix

Parameters of the DFIG:

Parameters	Value
Nominal power	$P_n = 4\ KW$
Stator voltage	$U_{sn} = 380\ V$
Rotor voltage	$U_{rn} = 220\ V$
Nominal current	$I_n = 15/8.6\ A$
Nominal mechanical speed	$\Omega_n = 1440\ rpm$
Nominal stator & rotor frequencies	$\omega_{sn} = 50Hz$
Pole pair number	$P = 2$
Stator resistance	$R_s = 1.2\ \Omega$
Rotor resistance	$R_r = 1.8\ \Omega$
Stator self inductance	$L_s = 0.1554\ H$
Rotor self inductance	$L_r = 0.1568\ H$
Mutual inductance	$M = 0.15\ H$
Moment of inertia	$J = 0.2\ Kg.m^2$
Friction coefficient	$f = 0.001\ IS$

Nomenclature:

s, r	Stator and rotor subscripts
d, q	Direct and quadrate Park subscripts
V, I, φ	Voltage/ Current/ Flux variables
R_s, R_r	Stator, rotor resistance
L_s, L_r	Stator, rotor inductance
T_s, T_r	Statoric and rotoric time-constant
θ_s, θ_r	Statoric and rotoric flux position
σ	Leakage factor
ω_s	Electrical stator frequency
ω	Mechanical rotor frequency
Ω	Mechanical speed
C_{em}	Electromagnetic torque
C_r	External load torque
ρ	Air density
R_T	Radius of turbine
C_p	Power cefficient
λ	Speed ratio
β	Pitch angle
P_s, Q_s	Active and reactive stator power
PWM	Pulse width modulation
IT2FSMC	interval type-2 fuzzy sliding mode control
DFIG	doubly fed induction generator

References

[1] R. Rouabhi, "Contrôle des puissances générées par un système éolien à vitesse variable basé sur une machine asynchrone double alimentée", *Doct. Thesis*, University of Batna, Algeria, 2016.

[2] A. Boyette, "Contrôle-commande d'une GADA avec système de stockage pour la production

éolienne", *Doct. Thesis*, University of Henry Poincaré, Nancy I, France, 2006.

[3] S. E. M. Ardjoun and M. Abid, "Commande par mode glissant flou d'un système eolien à base d'une génératrice asynchrone à double alimentation", *2ème Journées Internationales sur les Énergies Renouvelables et le Développement Durable*, Laghouat, Algeria, 2012.

[4] R. Rouabhi, R. Abdessemed, A. Chouder, and A. Djerioui, "Hybrid Backstepping control of a doubly fed wind energy induction generator", *The Mediterranean Journal of Measurement and Control*, Vol. 11, No. 1, pp. 367-376, 2015.

[5] F. Poitiers, T. Bouaouiche, and M. Machmoum, "Advanced control of a doubly-ded induction generator for wind energy conversion", *Electric Power Systems Research*, Vol. 79, No. 7, pp. 1085-1096, 2009.

[6] Y. Bekakra and D. B. Attous, "Speed and flux control for DFOC of doubly fed induction machine using sliding mode controller", *Acta Electrotechnica et Informatica*, Vol. 10, No. 4, pp. 75-81, 2010.

[7] D. Cherifi and Y. Miloud, "Hybrid Control Using Adaptive Fuzzy Sliding Mode Control of Doubly Fed Induction Generator for Wind Energy Conversion System", *Periodica Polytechnica Electrical Engineering and Computer Science*, Vol. 64, No. 4, pp. 374-381, 2020.

[8] Z. Boudjema, A. Meroufel, Y. Djerriri, and E. Bounadja, "Fuzzy sliding mode control of a doubly fed induction generator for wind energy conversion", *Carpathian Journal of Electronic and Computer Engineering*, Vol. 6, No. 2, pp. 7-14, 2013.

[9] M. Benmeziane, S. Zebirate, A. Chaker, and Z. Boudjema, "Fuzzy sliding mode control of doubly-fed induction generator driven by wind turbine", *International Journal of Power Electronics and Drive System*, Vol. 10, No. 3, pp. 1592-1602, 2019.

[10] Z. Boudjema, R. Taleb, A. Yahdou, and H. Kahal, "High order sliding mode control of a DFIM supplied by two power inverters", *Journal of Electronic and Computer Engineering*, Vol. 8, No. 1, pp. 23-30, 2015.

[11] A. Saidi and F. Naceri, "Comparative study between sliding mode controller and fuzzy sliding mode controller in a speed control for doubly fed induction motor", *4th International Conference on Control Engineering & Infonnation Technology*, Hammamet, Tunisia, 2016.

[12] H. Amimeur, D. Aouzellag, R. Abdessemed, and K. Ghedamsi, "Sliding mode control of a dual-stator induction generator for wind energy conversion systems", *Electrical Power and Energy Systems*, Vol. 42, No. 1, pp. 60-70, 2012.

[13] R. Rouabhi, R. Abdessemed, A. Chouder, and A. Djerioui, "Power quality enhancement of grid connected doubly-fed induction generator using sliding mode control", *International Review of Electrical Engineering*, Vol. 10, No. 2, pp. 266-276, 2015.

[14] Z. Song and K. Sun, "Adaptive backstepping sliding mode control with fuzzy monitoring strategy for a kind of mechanical system", *ISA Transactions*, Vol. 53, No. 1, pp. 125-133, 2014.

[15] M. Rapin and J. M. Noël, "Energie éolienne", Dunod, Paris, 2010.

[16] A. Herizi, A. Bouguerra, S. Zeghlache, and R. Rouabhi, "Backstepping control of a doubly-fed induction machine based on fuzzy controller", *European Journal of Electrical Engineering*, Vol. 20, No. 5-6, pp. 645-657, 2018.

[17] L. Djilali, H. C. Barragan, L. P. O. Ibarra, E. N. Sanchez, and A.G. Loukianov, "Neural Sliding Mode Control of a DFIG Based Wind Turbine with Measurement Delay", *IFAC-PapersOnLine*, Vol. 51, No. 13, pp. 456-461, 2018.

[18] W. Slotine and J. J. E. Li, "Applied nonlinear control", *Prence Hall*, USA, 1998.

[19] P. Lopez and A. S. Nouri, "Théorie Elémentaire Et Pratique de La Commande Par Les Régimes Glissants", *Springer*, 2006.

[20] A. Herizi, A. Bouguerra, S. Zeghlache, and R. Rouabhi, "Hybrid type-2 fuzzy sliding mode control of a doubly-fed induction machine (DFIM)", *AMSE Journals-IETA Publication, Advances in Modelling and Analysis C*, Vol. 74, No. 2-4, pp. 1-10, 2019.

[21] H. Hassani and J. Zarei, "Interval Type-2 fuzzy logic controller design for the speed control of DC motors", *Systems Science & Control Engineering*, Vol. 3, No. 1, pp. 266-273, 2015.

[22] J. M. Mendel, R. I. John, and F. Liu, "Interval type-2 fuzzy logic systems made simple", *IEEE Transactions on Fuzzy Systems*, Vol. 14, No. 6, pp. 808-818, 2006.

[23] J. Mendel, "Uncertain rule-based fuzzy logic systems: introduction and new directions", *Prentice-Hall*, 2001.

[24] Q. Liang and J. M. Mendel, "Interval type-2 fuzzy logic systems: theory and design", *IEEE Transactions on Fuzzy Systems*, Vol. 8, No. 5, pp. 535-550, 2000.

[25] O. Castillo and P. Melin, "A review on the design and optimization of interval type-2 fuzzy controllers", *Applied Soft Computing*, Vol. 12, pp. 1267-1278, 2012.

[26] R. Juan, O. Castillo, P. Melin, and A. R. Díaz, "A hybrid learning algorithm for a class of interval type-2 fuzzy neural networks", *Information Sciences*, Vol. 179, pp. 2175-2193, 2009.

[27] O. Castillo, M. Marroquín, P. Melin, F. Valdez, and J. Soria, "Comparative study of bio-inspired algorithms applied to the optimization of type-1 and type-2 fuzzy controllers for an autonomous mobile robot", *Information Sciences*, Vol. 192, pp. 19-38, 2012.